



Microstructural Changes in Grade 22 Ferritic Steel Clad Successively with Ni-Based and 9Cr Filler Metals

A study was conducted of the interface microstructure in a Grade 22 ferritic steel base metal weld clad with ENiCrFe-3 and P91 filler metals

BY R. ANAND, C. SUDHA, V. THOMAS PAUL, S. SAROJA, AND M. VIJAYALAKSHMI

ABSTRACT

This investigation demonstrates the effectiveness of using a nickel-based interlayer in preventing the formation of hard and soft zones during postweld heat treatment of Grade 22 ferritic steel weld clad with Grade 91 ferritic steel. Since carbon diffusion due to the activity gradient is responsible for the formation of the zones, a nickel-based interlayer (ENiCrFe-3) was introduced by welding to prevent carbon diffusion, thereby controlling the formation of hard and soft zones. Postweld heat treatment of weldments with 0.1-mm-thick interlayers was carried out at 1023 K for 1 and 15 h. In-

terfacial microstructure and microchemistry between Grade 22/ENiCrFe-3 and Grade 91/ENiCrFe-3 were investigated in detail using electron microprobe and transmission electron microscopy. Formation of a hard zone was not observed at the interface of the P91 steel and ENiCrFe-3 interlayer. However, presence of a zone of retained austenite ($\sim 6 \mu\text{m}$ in width) at the interface between Grade 22 and ENiCrFe-3 was confirmed. This zone did not show any systematic variation in width with postweld heat treatment schedule. Formation of retained austenite was understood based on nickel dilution across the interface during welding.

0.47C and Fe-19Cr-8Ni-0.09C steels, presence of a 50- μm -thick interlayer of spectrally pure nickel was found to have a retarding influence on carbon redistribution (Ref. 8). The retarding effect was found to be directly proportional to the thickness of the interlayer. Further, a nickel-based diffusion barrier between a corrosion-resistant steel (Fe-3%Si) and carbon steel was found to reduce the thickness of the carburized zone by a factor of almost three (Ref. 9). Several such studies are available suggesting the beneficial effect of nickel-based antidiffusion barriers (Refs. 10–13). Nickel was also the preferred filler metal in ferritic-ferritic transition joints since its thermal expansion coefficient ($14.9 \times 10^{-6} \text{ K}^{-1}$ for ENiCrFe-3) lies closer to that of a ferritic steel ($14 \times 10^{-6} \text{ K}^{-1}$ for Grade 22) (Ref. 14).

The microstructure that develops at the interface between a low-Cr ferritic steel and nickel-based filler metal in austenitic-ferritic and ferritic-ferritic transition joints has been extensively studied and debated. J. Barford et al. (Ref. 15) have reported dark etching “finger like” duplex structure ($\alpha+\gamma$) extending from the 2/4Cr side to the Inconel® weld metal side in high-temperature exposed joints. Uniaxial tensile tests and creep tests performed on such joints showed that these duplex structures do not pose serious problems during fracture. There is agreement among several authors (Refs. 16–20) that instead of a duplex structure, M_{23}C_6 and M_6C carbides precipitate at the weld interface. These carbides are together designated as Type I or II depending on the microstructural feature associated with them and distance from the interface. Type I carbides appear as a narrow, sharp, well-delineated feature close to the weld interface and Type II carbides appear as a relatively wider band ($\sim 50\text{--}100 \mu\text{m}$ from the interface) of fine precipitates. Type I carbides are found to be responsible for premature failure of the joints in service. This is attributed to the cavitation around

Introduction

Ferritic steels are the preferred structural materials for steam generator circuits of thermal and nuclear power plants due to their good high-temperature oxidation and corrosion resistance as well as moderate creep rupture strength (Ref. 1). In-service exposure or postweld heat treatment (PWHT) of ferritic steel dissimilar weldments often results in the formation of a carbon depleted “soft zone” in the low-Cr side and a precipitate-rich “hard zone” in the high-Cr side near the weld interface (Refs. 2, 3). Diffusion of carbon due to the activity gradient from low-Cr to high-Cr side was identified as the principal cause for the formation of the zones (Ref. 4). It has been recognized that formation of such deleteri-

ous zones at the weld interface leads to premature failure of the welds, well before their design life period.

A number of methods have been identified (Refs. 5–7) to prevent the formation of hard and soft zones in dissimilar joints: 1) introducing a diffusion barrier to carbon, 2) reducing the activity gradient by welding steels with graded Cr composition, and 3) reducing the carbon activity on the low-Cr side by alloying with elements like Nb, V, or Ti, which have higher affinity for carbon. Of these methods, introduction of a nickel-based diffusion barrier was found to be most effective. In dissimilar weldments of Fe-

KEYWORDS

Cr-Mo Steels
Diffusion Barrier
Hard Zone Formation
Elemental Redistribution
Dissimilar Metal Welding

R. ANAND is a research scholar and C. SUDHA, V. THOMAS PAUL, S. SAROJA (saroja@igcar.gov.in), and M. VIJAYALAKSHMI are scientific officers with Physical Metallurgy Div., Metallurgy and Materials Group, Indira Gandhi Centre for Atomic Research, Kalpakkam, India.

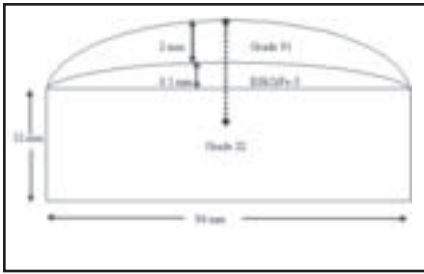


Fig. 1 — Schematic representation of the weld cladding under study (region of interest is marked by dotted lines).

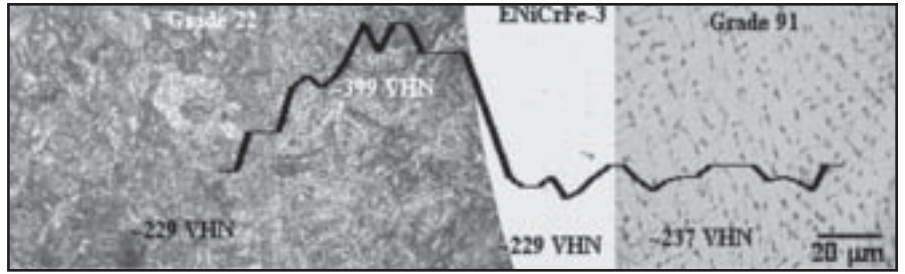


Fig. 2 — Optical microstructure and superimposed hardness profile across as-received weld cladding of Grade P91 on Grade 22 ferritic steel with 0.1-mm-thick ENiCrFe-3 interlayer.

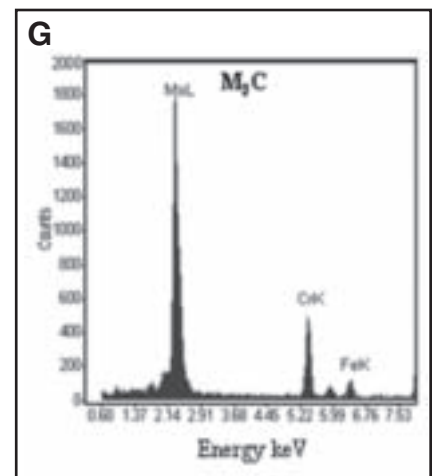
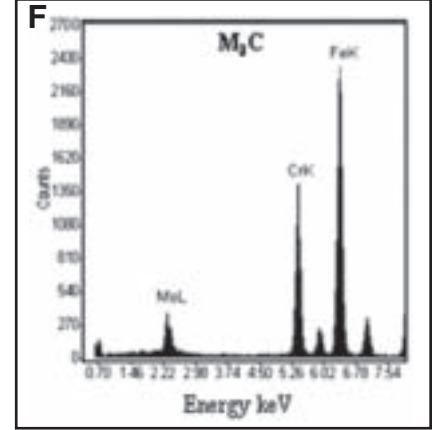
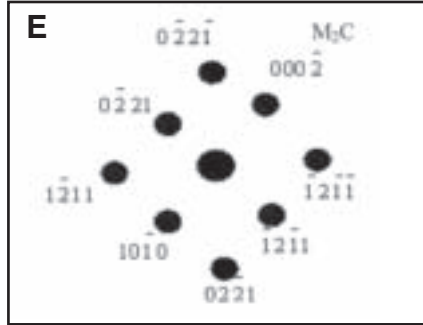
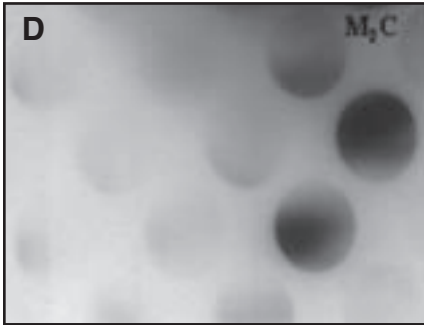
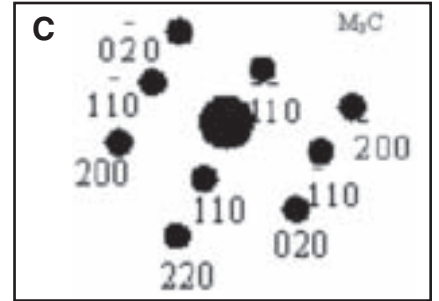
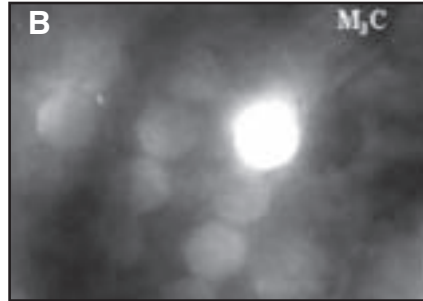
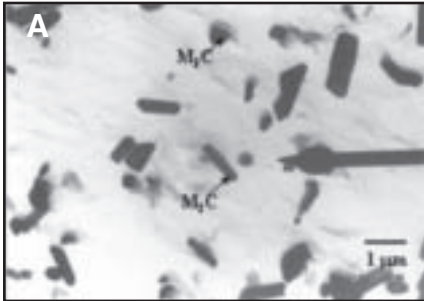


Fig. 3 — A — TEM micrograph showing the presence of globular M_3C - and acicular M_2C -type of precipitates in Grade 22 base material of as-received weld cladding; B — micro diffraction pattern along $\langle 001 \rangle$ zone axis for M_3C -type of precipitate; C — corresponding key for the micro diffraction pattern; D — micro diffraction pattern along $\langle 0110 \rangle$ zone axis for M_2C -type of precipitates; E — corresponding key for the micro diffraction pattern; F — EDS spectra showing Fe enrichment in M_3C -type of precipitate; G — Mo enrichment in M_2C -type of precipitate.

Table 1 — Chemical Composition of the Base Metal and Electrodes

| Description | Element (wt-%) | | | | | | | | | |
|----------------------------------|----------------|-------|------|------|-------|------|------|----|------|-----|
| | C | Cr | Mo | Mn | S | P | Si | Ni | Nb | Ti |
| Grade 22 (ASTM A387) | 0.12 | 2.18 | 1.0 | 0.46 | 0.001 | 0.01 | 0.25 | — | — | — |
| Grade 91 (Electrode) (ASTM A387) | 0.08 | 10.25 | 0.98 | 0.91 | 0.02 | 0.02 | 0.40 | — | — | — |
| ENiCrFe-3 (Electrode) | 0.05 | 13.8 | — | 7.84 | 0.004 | 0.01 | 0.56 | 66 | 1.84 | 0.4 |

Table 2 — Welding Parameters Used for the Preparation of Weld Cladding

| Base Metal | Electrode | Electrode Diameter (mm) | Current (A) | Voltage (V) | Speed (mm/min) | Preheat (°C) |
|------------|-----------|-------------------------|-------------|-------------|----------------|--------------|
| Grade 22 | ENiCrFe-3 | 3 | 80 | 22 | 140 | 150 |
| ENiCrFe-3 | Grade 91 | 5 | 80 | 22 | 140 | — |

the carbide particles leading to interfacial crack propagation (Refs. 21, 22). Investigation on the crack propagation in power plant boilers after service at 838 K from 40,000 to 200,000 h revealed that these carbide precipitates redissolve when heated above 977 K (Ref. 23).

Despite all these observations con-

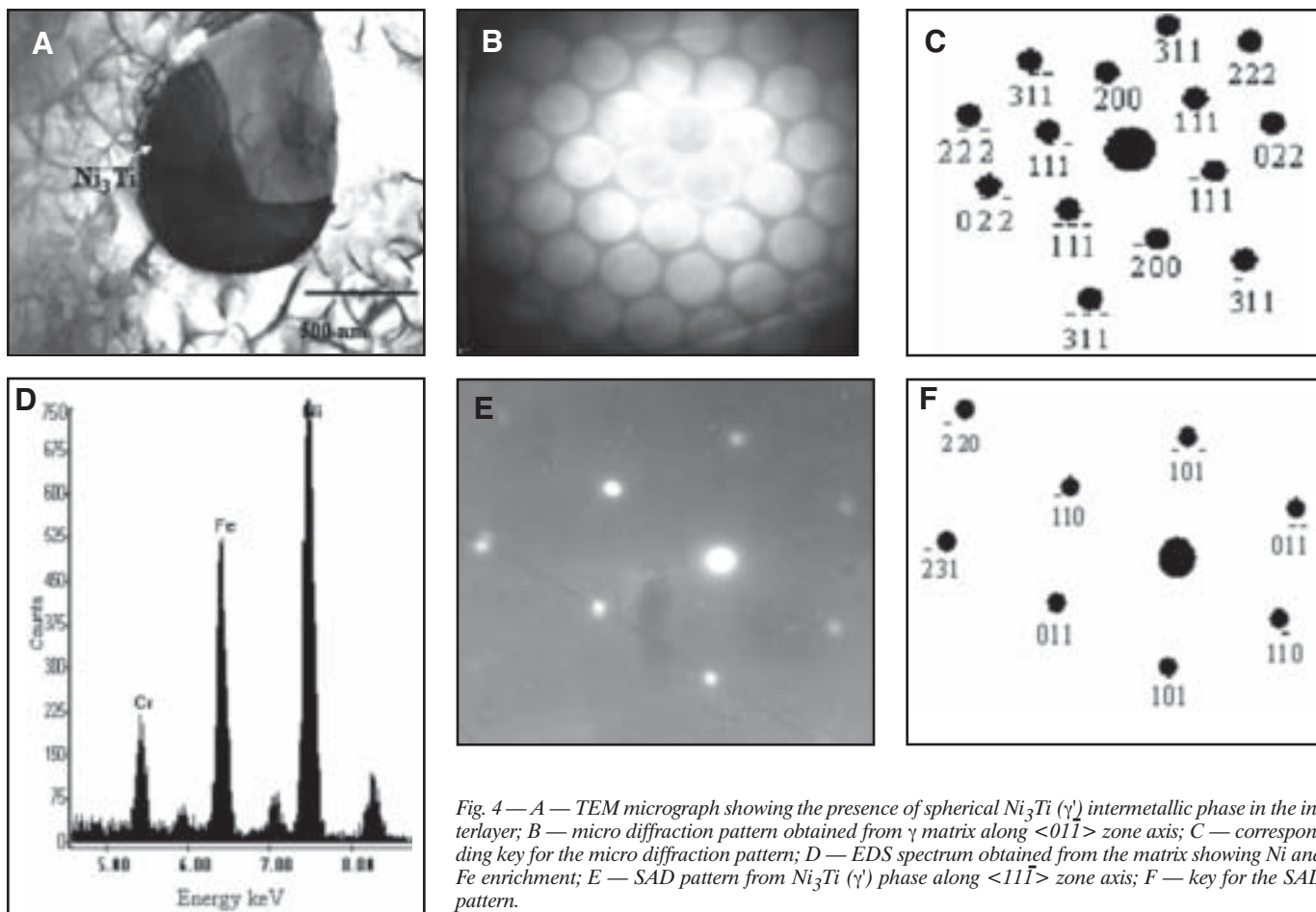


Fig. 4 — A — TEM micrograph showing the presence of spherical Ni_3Ti (γ') intermetallic phase in the interlayer; B — micro diffraction pattern obtained from γ matrix along $\langle 01\bar{1} \rangle$ zone axis; C — corresponding key for the micro diffraction pattern; D — EDS spectrum obtained from the matrix showing Ni and Fe enrichment; E — SAD pattern from Ni_3Ti (γ') phase along $\langle 11\bar{1} \rangle$ zone axis; F — key for the SAD pattern.

cerning the interfacial microstructure between Grade 22 ferritic steel and nickel-based filler material, there is a universal agreement that the nickel-based interlayer reduces the peak hoop stress of the weld joint by about 38% (Refs. 24, 25). No failures were reported in Grade 22/Ni-17Cr-6Fe-0.1C joints even after being in service for 15 years (Ref. 26). Nickel-based interlayers are still considered to be the best choice to reduce carbon diffusion in dissimilar weldments of ferritic and austenitic steels (Refs. 27–29).

The authors have carried out extensive investigations on the formation of hard and soft zones in direct dissimilar weldments of 9Cr-1Mo/2¼Cr-1Mo ferritic steels (Refs. 5, 30). Numerical simulations based on the finite difference method predicted that an $\sim 80\text{-}\mu\text{m}$ -thick nickel-based diffusion barrier is sufficient to prevent the formation of the zones (Refs. 31, 32). In the present study, the above prediction has been experimentally verified by introducing an $\sim 100\text{-}\mu\text{m}$ -thick nickel-based interlayer in dissimilar joints of ferritic steels. The effectiveness of using ENiCrFe-3 filler metal in preventing the formation of hard and soft zones in ASTM A387 Grade 91 weld cladding

on ASTM A387 Grade 22 ferritic steel has been investigated. Detailed microstructural and microchemical characterization has been carried out using electron microprobe and analytical transmission electron microscopy analysis.

Experimental Details

Weld cladding was performed by shielded metal arc welding (SMAW) on Grade 22 base metal using ENiCrFe-3 and Grade 91 electrodes successively. Grade 22 base metal prior to welding was in the normalized and tempered condition. Composition of Grade 22, Grade 91, and ENiCrFe-3 are given in Table 1 and the welding parameters are listed in Table 2. Thickness of the ENiCrFe-3 interlayer between the ferritic steels was restricted to 0.1 mm. Figure 1 shows the schematic representation of the weld cladding used for the present investigation, where the region of interest is marked by dotted lines.

The welded specimens were given PWHT at 1023 K for 1 and 15 h. The weldments were polished using conventional metallographic procedure and etched using Vilella's reagent for microstructural examination. Easier observation of ENi-

CrFe-3/ferritic steel interface was facilitated by using an etchant only for the ferritic steels. A specific etchant for retained austenite, 30% glycerol-10% HNO_3 -20% HCl was used to reveal the structure at Grade 22/ENiCrFe interface. Microstructural examination was carried out using an optical microscope (model No: MEF4A of M/s Leica) and scanning electron microscope (XL 30 ESEM of M/s FEI), which was attached with an energy-dispersive spectrometer (EDS). A Leitz microhardness tester with an applied load of 100 g was used for microhardness measurements. An X-ray diffractometer (XRG3000 model of M/s INEL) equipped with a curved position-sensitive detector was used to identify different phases present in Grade 91 filler metal and at the interface of Grade 22/ENiCrFe-3. $\text{Cu K}\alpha$ was used as the incident radiation at 40 kV and 30 mA. Angular 2θ range from 10 to 90 deg was covered with a step size of 0.012 deg.

Elemental distribution across the weld interface between Grade 22/ENiCrFe-3 and Grade 91/ENiCrFe-3 was identified using a Cameca SX50 electron probe micro analyzer (EPMA). Accelerating voltage of 20 kV and beam current of 20

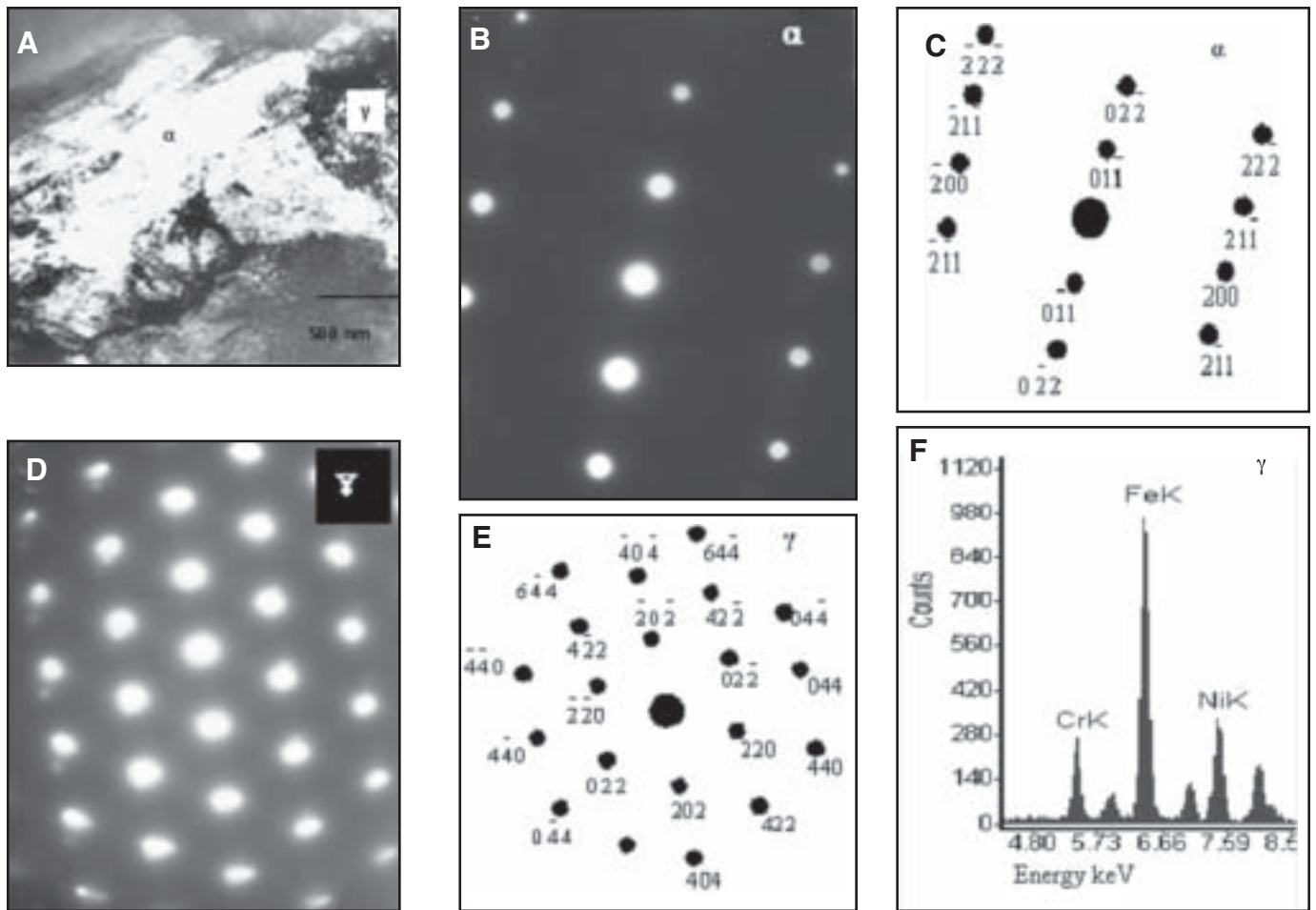


Fig. 5 — A — TEM micrograph obtained from Grade 91 ferritic steel showing the presence of both ferrite (α) and austenite (γ) phases; B — SAD pattern obtained from α phase along the $\langle 01\bar{1} \rangle$ zone axis; C — key for the SAD pattern; D — SAD pattern obtained from γ phase along $\langle 11\bar{1} \rangle$ zone axis; E — key for the SAD pattern; F — EDS spectrum obtained from the γ phase showing the presence of Ni.

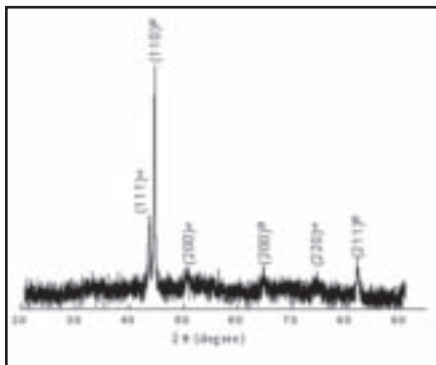


Fig. 6 — X-ray diffraction pattern showing the presence of both α (ferrite) and γ (austenite) phases in Grade 91 steel of as-received weld cladding.

nA were used for the analysis of iron, chromium, and nickel, whereas 10 kV and 20 nA were used for the analysis of carbon. Crystals used were LiF for Fe $K\alpha$, Cr $K\alpha$, and Ni $K\alpha$, and PC2 for C $K\alpha$. Quantitative analysis was performed by comparing the intensities of $K\alpha$ or $L\alpha$ radiation of the elements obtained from the sample with that of the standards. A specialized computer package was used for quantita-

tive analysis, which takes care of the corrections to be made while calculating the concentrations of various elements.

Base metal, weld metal, as well as the weld interface were analyzed using a Philips CM 200 analytical transmission electron microscope (TEM) with an energy-dispersive spectrometer (EDS) with a superultra-thin window. Thin foils as well as carbon extraction replicas were used in the investigation. To prepare the carbon extraction replicas, initially the samples were polished to a mirror finish and etched using Vilella's reagent. The entire specimen except the specific region to be studied was then masked with thin Al foil. After carbon coating, the Al foil was removed and again the sample was etched using Vilella's reagent. On etching, the carbon film with extracted carbides could be removed from the region of interest and collected in Cu mesh for TEM analysis.

To prepare thin foils of Inconel interlayer and 9Cr-1Mo weld bead, these portions were cut from the weld cladding. The samples were initially mechanically polished using silicon carbide papers up to a thickness of $\sim 100 \mu\text{m}$. Then 3-mm discs were punched out of these polished spec-

imens. To get electron transparent material the 3-mm discs were further polished by jet thinning technique using 20% perchloric acid+10% methanol as electrolyte at a temperature of 258 K. Selected area diffraction (SAD) or micro diffraction patterns were used to get crystallographic information and EDAX spectra were used to get information about microchemistry, as given in the Appendix.

Results

Characteristics of As-Received Weld Cladding

Figure 2 shows the optical microstructure and superimposed hardness profile of the as-received weld cladding. Grade 22 ferritic steel showed a bainitic structure, while the Grade 91 ferritic steel exhibited a solidification structure. ENiCrFe-3 was not etched by the Vilella's reagent. Average hardness of 229 VHN was obtained on Grade 22 base plate and ENiCrFe-3 weld bead. Heat-affected zone (HAZ) on the base metal side showed a high hardness of ~ 399 VHN. Hardness values of around

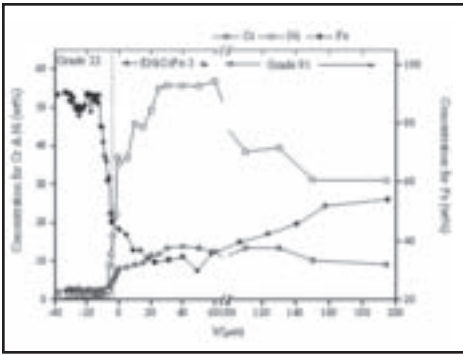


Fig. 7 — EPMA concentration profiles for Cr, Ni, and Fe as a function of distance x from the interface for as-received weld cladding.

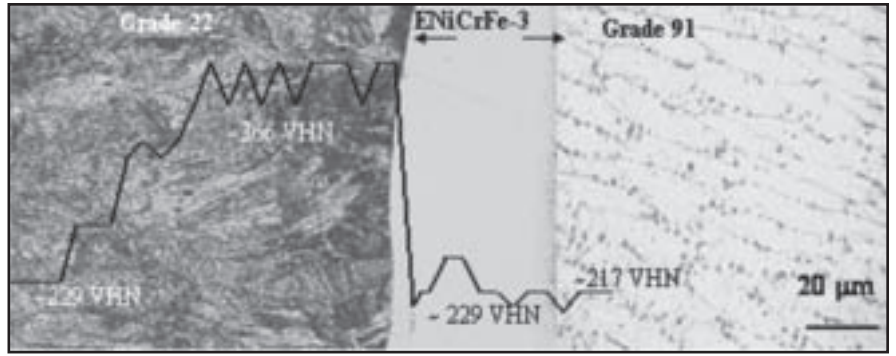


Fig. 8 — Optical microstructure and superimposed hardness profile across a weld cladding of Grade 91 on Grade 22 ferritic steel with 0.1-mm-thick ENiCrFe-3 interlayer subjected to PWHT at 1023 K for 1 h showing no change from as-received condition.

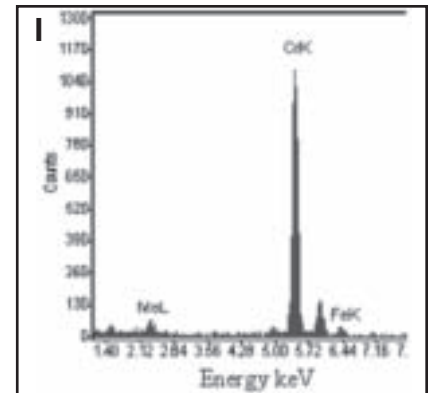
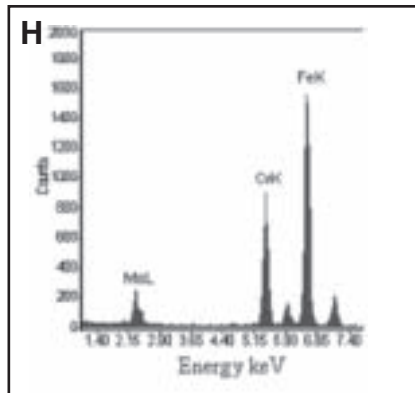
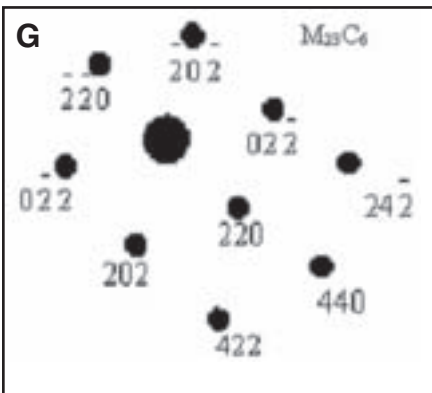
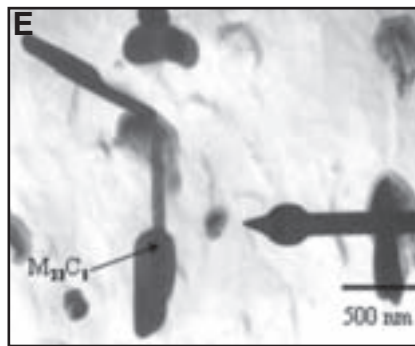
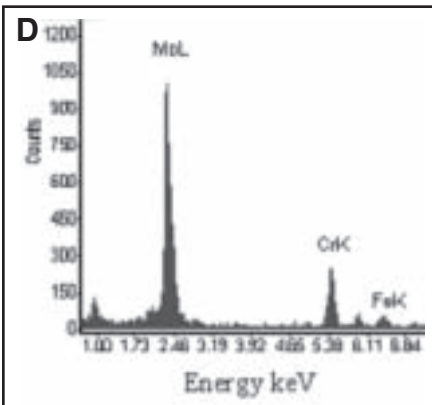
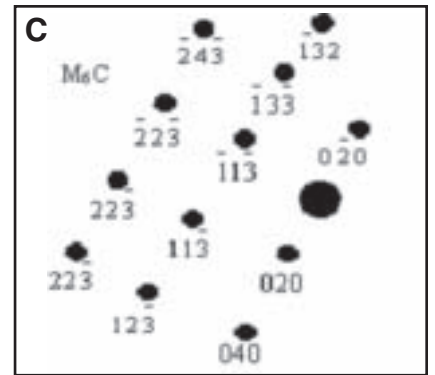
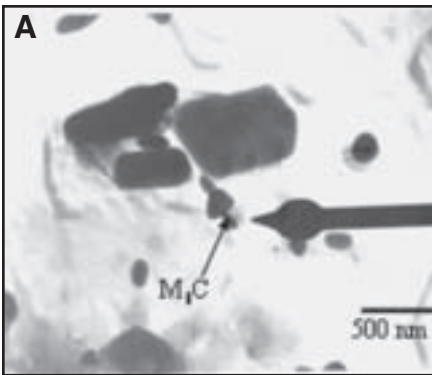


Fig. 9 — TEM micrographs, electron diffraction patterns, and EDS spectra obtained from Grade 22 base metal after PWHT at 1023 K for 15 h showing the following: A — Needle-shaped M_6C -type precipitate; B — micro diffraction pattern from M_6C precipitate along $\langle 301 \rangle$ zone axis; C — key for the micro diffraction pattern; D — EDS spectrum showing Mo enrichment in M_6C precipitate; E — TEM micrograph showing bulky $M_{23}C_6$ -type precipitate; F — SAD pattern from $M_{23}C_6$ precipitate along $\langle 111 \rangle$ zone axis; G — key for the SAD pattern; H and I — EDS spectra showing Fe and Cr enrichment in $M_{23}C_6$ precipitate, respectively.

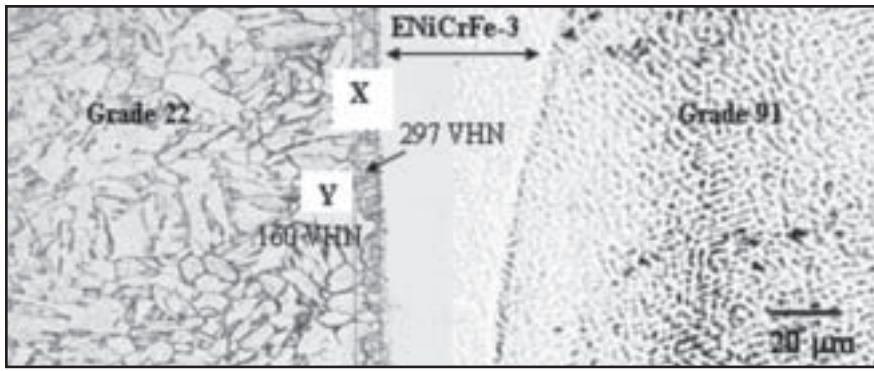


Fig.10 — Optical microstructure of weld cladding after PWHT at 1023 K for 15 h showing microstructural modification (marked as X and Y) in Grade 22/ENiCrFe-3 interface.

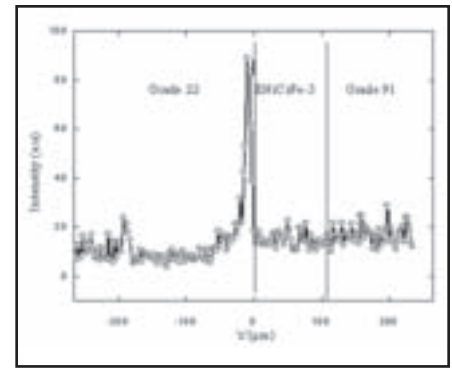


Fig.11 — X-ray intensity profile across the weld cladding after PWHT at 1023 K for 15 h showing carbon enrichment in the dark etching region X near the Grade 22/ENiCrFe-3 interface.

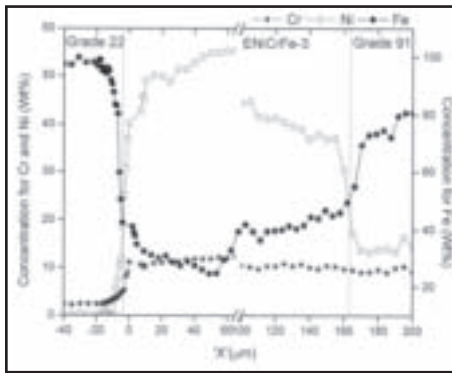


Fig. 12 — EPMA concentration profiles for Fe, Ni, and Cr as a function of distance x from the interface after PWHT at 1023 K for 15 h.

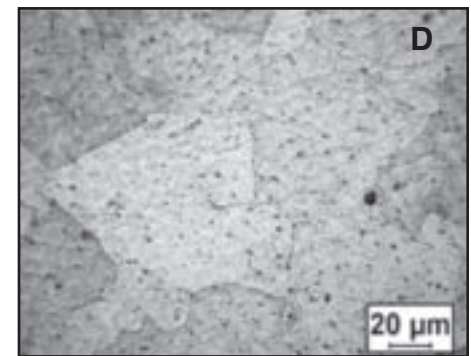
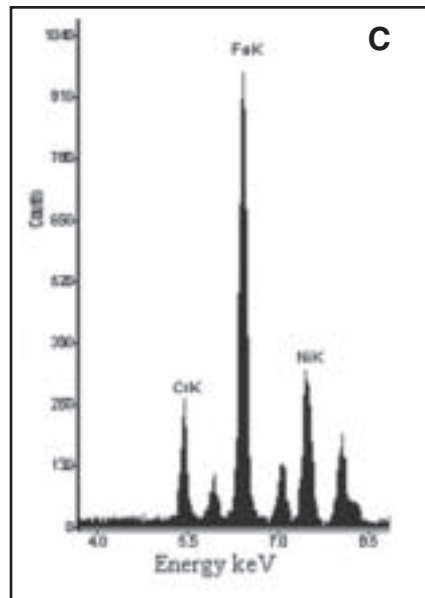
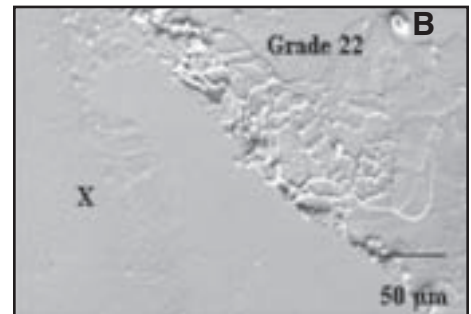
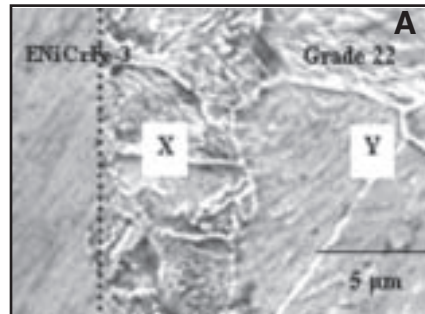


Fig. 13 — SEM micrograph showing the following: A — Cross section of the weld cladding subjected to PWHT at 1023 K for 15 h where the dark etched band is marked as X and ferrite grains are visible in Y; B — interface between X and Grade 22 steel as observed from the surface of the specimen cut along dotted lines as indicated in A; C — EDS spectrum obtained from X showing the presence of Ni; D — optical micrograph revealing retained austenite structure of X.

237 VHN only were obtained on Grade 91 ferritic steel, which were consistent with the observed microstructure.

Figure 3 shows the TEM micrographs and electron micro diffraction patterns, as well as EDS spectra obtained from Grade 22 base metal. Figure 3A shows the presence of both globular M_3C and acicular M_2C type of precipitates in the base metal. Analysis of the micro diffraction patterns given as Fig. 3B and D showed that the globular M_3C -type of precipitate is along $\langle 001 \rangle$ zone axis and acicular M_2C precipitate is along the $\langle 01\bar{1}0 \rangle$ zone axis, respectively. M_3C precipitates are Fe rich and M_2C precipitates are all Mo rich as shown in the EDS spectra given as Fig. 3F and G, respectively.

Figure 4A shows the TEM micrograph obtained from the ENiCrFe-3 interlayer, which shows the presence of an intermetallic phase in the matrix. From the analysis of the micro diffraction pattern (Fig. 4B), the matrix was found to have austenite structure with the orientation along the $\langle 01\bar{1} \rangle$ zone axis. The EDS spectrum (Fig. 4D) obtained from the matrix showed higher Fe content than what is expected from the composition of the interlayer. From the analysis of the SAD pattern given in Fig. 4E, the secondary phase existing in the matrix was identified

as Ni_3Ti (γ') intermetallic phase. The intermetallic phase exhibited a spherical morphology and the orientation was found to be along $\langle 11\bar{1} \rangle$ zone axis. EDS spectrum could not be obtained from the intermetallic phase due to matrix interference. Figure 5A shows the TEM micrograph obtained from Grade 91 ferritic steel showing a contrast difference, suggesting a two-phase structure. Analysis of the SAD patterns (Fig. 5B and D) obtained from the two regions showed the presence of both ferrite (α) and austenite (γ) phases along $\langle 01\bar{1} \rangle$ and $\langle \bar{1}11 \rangle$ zone axes, respectively. The EDS spectrum

(Fig. 5F) obtained from the γ phase showed the presence of $\sim 29\%$ Ni. To further confirm the presence of γ phase on the Grade 91 side X-ray diffraction pattern (Fig. 6) was obtained. The XRD spectrum showed the presence of (111), (200), and (220) peaks corresponding to γ phase as well as (110), (200), and (211) peaks corresponding to α phase. Lattice parameter for the γ phase was obtained as $3.5891 \pm 0.003 \text{ \AA}$ and for α phase as $2.8715 \pm 0.004 \text{ \AA}$.

To determine elemental distribution across the weld interface, quantitative X-ray intensity measurements were obtained

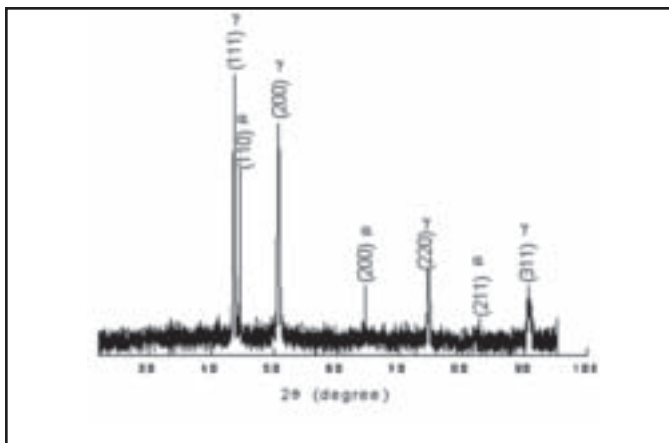


Fig. 14 — X-ray diffraction pattern confirming the presence of retained austenite in the dark-etched band X present in Grade 22/ENiCrFe-3 interface.

using an electron microprobe — Fig. 7. Within $\sim 6 \mu\text{m}$ distance on the Grade 22 side of the Grade 22/ENiCrFe-3 interface, Ni content decreased from 20 wt-% near the interface to 0% corresponding to the base metal. Cr concentration changed from about 10 wt-% near the weld interface to 2.25% corresponding to the base metal. However, across the Grade 91/ENiCrFe interface, significant distribution of the alloying elements was observed. On the ENiCrFe-3 side, nickel content decreased from 66 to 40% and iron content increased from 8 to 15%. Similar observation was also made on the Grade 91 side where the Fe content was found to have decreased from 90 to 66%, whereas the nickel content increased from 0 to 30%.

Effect of PWHT on Weld Cladding

Figure 8 shows the optical microstructure of the weld cladding after PWHT at 1023 K for 1 h. Grade 22 showed tempered bainitic structure and Grade 91 retained the solidification structure. Superimposed hardness profile shows a hardness value of 366 VHN in the HAZ and 212 VHN in Grade 22 base metal. Average hardness value of 225 VHN was obtained on ENiCrFe-3 and Grade 91. No observable microstructural change could be seen either in Grade 22/ENiCrFe or in Grade 91/ENiCrFe interface.

After 15 h of heat treatment, Grade 22 showed predominantly a ferrite structure with limited retention of bainite in the base metal away from the interface. Figure 9 shows the TEM micrographs, electron diffraction patterns as well as EDS spectra obtained from Grade 22 base metal. Both M_6C - and $M_{23}C_6$ -types of precipitates were detected. The M_6C -type precipitate had needle-shaped morphology (Fig. 9A) with orientation along $\langle 30\bar{1} \rangle$ zone axis (Fig. 9B). It was also found to be Mo rich as shown by the EDS

spectrum in Fig. 9D. The $M_{23}C_6$ precipitates were globular (Fig. 9E) along $\langle \bar{1}11 \rangle$ zone axis (Fig. 9F). Both Fe- and Cr-rich $M_{23}C_6$ precipitates were detected, as shown by the EDS spectra in Fig. 9H and I, respectively. Even after 15 h of heat treatment, 9Cr-1Mo retained the solidification structure. An overall reduction in the hardness of the weldment was observed.

Microstructural modification was not observed in Grade 91/ENiCrFe interface after 15 h of heat treatment — Fig. 10. Electron microscopy studies carried out on carbon replicas extracted from the interface of Grade 91/ENiCrFe showed no evidence of the presence of carbide precipitates. This is in sharp contrast to the behavior that had a hard zone formed. In Grade 22 and ENiCrFe-3 interface, a dark etched zone of $\sim 6 \mu\text{m}$ width (marked as X in Fig. 10) and a light etched region of $\sim 20 \mu\text{m}$ width (marked as Y in Fig. 10) were observed. Average hardness of 289 VHN on X and ~ 152 VHN on Y was obtained. The X-ray elemental line scan for carbon (Fig. 11) obtained using an electron microprobe showed increase in carbon intensity corresponding to X. Quantitative elemental analysis across the weld interface using electron microprobe (Fig. 12) showed that variation of Ni, Cr, and Fe

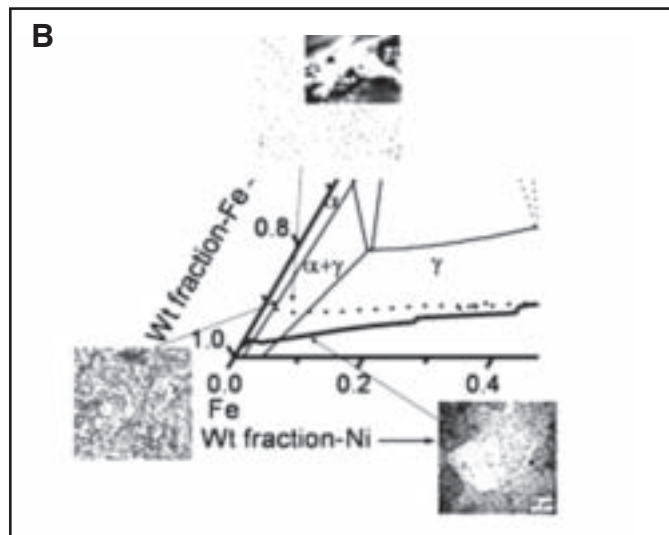
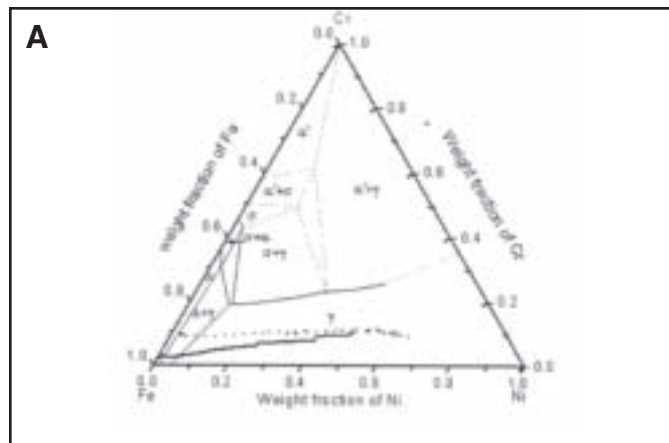


Fig. 15 — A — Schematic of the Fe-Cr-Ni ternary phase diagram at 1073 K with superimposed diffusion profiles obtained across the Grade 22/ENiCrFe-3 interface (solid lines) and Grade 91/ENiCrFe-3 interface (dotted lines) for weld cladding PWHT at 1023 K for 15 h. Diffusion profiles show the existence of γ and $\alpha+\gamma$ phases in the Grade 22/ENiCrFe-3 interface and dual phase ($\alpha+\gamma$) structure in Grade 91; B — expanded portion of the phase diagram with microstructures of corresponding phase fields inserted.

concentration across Grade 91/ENiCrFe-3 interface as well as Grade 22/ENiCrFe-3 interface was similar to that in as-received joints. No redistribution for chromium was observed between X and Y.

Figure 13A shows possibly a dual-phase structure of X and ferrite grains in Y. To further investigate the dark etching band X, a cross section of the weld was cut parallel to the Grade 22/ENiCrFe-3 interface (marked by dotted lines in Fig. 13A). The cut surface (Fig. 13B) was repeatedly polished and etched till the area fraction of X was $\sim >0.5$. EDS spectrum given as Fig. 13C shows the presence of Ni in the dark etching band X. Figure 13D shows the retained austenite structure of the dark etching band X, which was revealed only after using a special etchant for retained austenite. Further confirmation for the presence of retained

austenite in X was obtained using X-ray diffraction pattern (Fig. 14), which showed the presence of (111), (200), and (220) peaks corresponding to the γ phase and (110), (200), and (211) peaks corresponding to the α phase.

Discussion

In the as-received weld cladding, Grade 22 base material, which was in the normalized and tempered condition, exhibited a bainitic structure with a hardness value of around 229 VHN. In the HAZ, a high hardness value of around 399 VHN was obtained (Fig. 2). During welding, the base material, which is directly in contact with the weld metal, can experience temperatures above A_3 (temperature at which transformation from ferrite to austenite is complete). Depending upon the cooling rate, the austenite can transform to martensite or bainite. A high hardness value of around 399 VHN is indicative of a martensitic transformation in the HAZ during cooling subsequent to welding. Electron microscopy investigations carried out on the carbon extraction replicas obtained from the base metal showed the presence of Fe_3C and Mo_2C type of precipitates — Fig. 3. This is in accordance with the reported microstructure of normalized and tempered Grade 22 steel (Ref. 33).

After PWHT for 1 h, a slight reduction in the overall hardness of the weld cladding was noticed as a result of tempering of the microstructure. Otherwise no significant change in the microstructure was observed after 1 h of heat treatment — Fig. 8. When the PWHT duration was increased to 15 h, the microstructure of Grade 22 base metal showed predominantly a ferrite structure with limited retention of bainite — Fig. 10. The presence of bulky globular Fe or Cr-rich $M_{23}C_6$ and needle-shaped Mo-rich M_6C were confirmed through electron microscopy investigations — Fig. 9. The microstructure obtained was similar to that of high-temperature (1023 K) exposed Grade 22 steel containing 0.11% C (Ref. 34).

Microstructure of ENiCrFe-3 interlayer in as-received weld cladding (Fig. 4) showed the presence of Ni_3Ti (γ') intermetallic phase in γ matrix. This observation is in accordance with the microstructure observed for nickel-based superalloys (Ref. 35). On the Grade 91 side, a solidification structure was obtained both in as-received and PWHT weld cladding — Figs. 2, 8, and 10. Electron microscopy investigations did not reveal the presence of carbides on the Grade 91 side after heat treatment. From electron microprobe investigation (Fig. 7), it is found that considerable redistribution of the alloying elements had taken place be-

tween Grade 91 ferritic steel and ENiCrFe-3 interlayer due to mixing during welding. On the Grade 91 side, the Ni content was found to be quite high (30 wt-%). It is expected that the high Ni content near the weld interface on Grade 91 side would favor the formation and retention of γ phase during cooling subsequent to welding. Confirmation for the existence of γ phase on Grade 91 was obtained both from electron microscopy and X-ray diffraction analysis — Figs. 5 and 6. Since these investigations were performed on the cross section of the weld overlay, the α phase also was detected along with γ . Volume fraction of γ phase in Grade 91 can be calculated using the following formula (Ref. 36)

$$\frac{I_\gamma}{I_\alpha} = \frac{R_\gamma V_\gamma}{R_\alpha V_\alpha} \quad (1)$$

and

$$V_\gamma + V_\alpha = 1 \quad (2)$$

where V_γ and V_α are volume fraction of the austenite and ferrite phase, respectively, I_γ and I_α are measured integrated intensity of (111) and (200) peaks for γ and (110) and (200) peaks for α phase, respectively. R_γ and R_α are constants calculated from crystal structure and lattice parameters for both phases as follows

$$R = \left(\frac{1}{v^2} \right) \left[|F|^2 p \left(\frac{1 + \cos^2 2\theta}{\sin^2 \theta \cos \theta} \right) \right] e^{-2M} \quad (3)$$

where v is the volume of the unit cell (m^3), F is the structure factor, p is the multiplicity factor, θ is the Bragg angle, and e^{-2M} is the temperature factor. Using the above formulas, volume fraction of the γ phase in Grade 91 steel is found to be 0.38 and that of the α phase is 0.62. High Ni content in Grade 91 will expand the γ phase field and also reduce the martensitic start (Ms) temperature considerably. The effect of Ni on Ms temperature was evaluated based on Andrews (linear) equation (Ref. 37) given below where the concentration of the alloying elements are expressed in wt-%.

$$Ms(^{\circ}C) = 539 - 423C - 30.4Mn - 12.1Cr - 17.7Ni - 7.5Mo \quad (4)$$

On substituting the concentration of alloying elements in Grade 91 filler metal, the Ms temperature is obtained as 137 K, which is much below the room temperature. In a recent work in literature (Ref. 38), the following empirical equation based on neural network analysis has been suggested for accurate determination of the Ms temperature of steels.

$$Ms(K) = 765.2 - 302.6C - 30.6Mn - 16.6Ni - 8.9Cr + 2.4Mo - 11.3Cu + 8.58Co + 7.4W - 14.5Si \quad (5)$$

Input variables for the neural network were obtained from a range of elemental concentration (e.g., C 0.001 to 1.62%, Mn 0 to 3.76%, Cr 0 to 17.9%, Ni 0 to 27.2%, Mo 0 to 5.10%). Ms temperature for Grade 91 filler metal calculated using the above equation agreed well with the value obtained using Andrews equation. The martensitic start temperature reported in the literature (Ref. 39) for 9Cr-1Mo steel having 8.25%Cr is below 673 K. Hence, the presence of Ni in Grade 91 would have drastically reduced the Ms temperature as a consequence of which the martensitic transformation is completely suppressed on cooling subsequent to welding. This explains the solidification structure with very low hardness than what is expected on Grade 91 side in as-received weld cladding.

Such a change in the structure of Grade 91 steel is brought about due to mixing during welding. Since the melting point of ENiCrFe-3 (1369–1673 K) is close to that of Grade 91 ferritic steel (1281–1473 K), it is possible that during deposition of Grade 91 bead, the underlying ENiCrFe bead would also have melted or heated to high temperature leading to mixing of the molten material. No zone or formation of intermetallics was observed at the interface of Grade 91 and ENiCrFe-3. Even otherwise, the interface between a high-Cr ferritic steel/Ni-based interlayer is considered to be less problematic when compared to low-Cr ferritic steel/Ni-based interlayer since the low-carbon activity gradient at the interface inhibits carbon diffusion. It has been reported (Ref. 20) that in single V-groove butt joint welds of Alloy 800 (Fe-31Ni-20Cr-0.03C) and Grade 91 steel, because of the low-carbon activity in the Grade 91 ferritic steel, only limited precipitation is observed at the interface after prolonged aging. An increase in the Ni content in the filler metal may further limit this precipitation.

In the interface of Grade 22 and ENiCrFe-3, the dark-etched region of $\sim 6\text{-}\mu\text{m}$ thickness observed after PWHT at 1023 K for 15 h (marked as X in Figs. 10 and 13A) was identified as retained austenite. The adjacent light-etched region of $\sim 20\text{-}\mu\text{m}$ thickness (marked as Y in Figs. 10 and 13A) was identified as ferrite. Reason for the formation of dark etching zone X can be understood as follows:

Electron microprobe based investigations showed high concentration for Ni and Cr, from the interlayer to $\sim 6\text{-}\mu\text{m}$ distance into the Grade 22 side of the interface, which may be a result of dilution of the base metal during welding. Concen-

tration of Ni in Grade 22 very near the interface was 20 wt-% and that for Cr was 10%. From the structure diagram for Cr-Ni steels proposed by Strauss and Maurer (Ref. 40) for the given concentration of Ni and Cr, only γ phase is expected to form very near the weld interface. In addition to stabilizing the γ phase field, presence of Ni also brings down the Ms temperature to 265 K (from Equation 4). Hence, a retained austenite structure is expected to form very near the interface between Grade 22 and ENiCrFe-3. Evidence for the existence of retained austenite was obtained in such weldments — Figs. 13, 14. As the distance from the interface increases on Grade 22, Ni and Cr contents decreased gradually to reach the base material concentration beyond 6 μm . Hence, it is to be expected that the zone X will have dual-phase structure with the ratio of the volume fraction of α to that of γ increasing with distance from the interface.

In an earlier work (Ref. 15) on dissimilar joints between Grade 22 and Inco-A, presence of dark etching fingers have been reported. This feature was found to be absent in the as-welded specimens, and even in heat-treated joints they were not found throughout the weld interface. Formation of such zones was related to degeneration of martensite during heat treatment. In the present work, the dark etching zone X also was not observed in the as-received weld cladding, but it was present throughout the weld interface in heat-treated specimens. However, evidence was obtained (Fig. 7) for the redistribution of alloying elements during welding up to $\sim 6\text{-}\mu\text{m}$ distance in the base metal, which confirms the existence of the zone in the as-received specimen also. Since this zone of very small thickness is present adjacent to a dark etching HAZ of the base metal, observing it as a well-defined feature with a sharp interface is difficult.

Figure 15A shows the schematic of Fe-Cr-Ni ternary phase diagram at a temperature of 1073 K. The diffusion profiles across Grade 22/ENiCrFe-3 and Grade 91/ENiCrFe-3 interfaces are superimposed on the phase diagram. Figure 15B shows an expanded portion of lower Ni-higher Fe section of the phase diagram with microstructures of corresponding phase fields superimposed. It is clear from Fig. 15A that the composition on Grade 91 side exists in $\alpha+\gamma$ phase field. As a result of this, it exhibits a dual-phase solidification structure, evidence for which is given in Fig. 15B. Again from Fig. 15A, it is seen that in the Grade 22/ENiCrFe-3 interface on the Grade 22 side, the γ phase field exists up to some distance after which the structure changes from γ to $\alpha+\gamma$. Evidence for these observations are also given in Fig. 15B.

The formation of an additional zone Y adjacent to X after heat treatment for 15 h can be explained as follows:

Formation of retained austenite (in X) during welding introduces an α/γ interface (between base material and X) within Grade 22 ferritic steel, thereby introducing a carbon activity gradient. PWHT would have led to the diffusion of carbon from the Grade 22 side to the zone X. Using an electron microprobe carbon enrichment has been observed in the region corresponding to X — Fig. 11. Since the solubility of carbon in γ phase is much higher than that in ferritic steel, no precipitation is observed. Also, since carbon is an austenite stabilizer it would have further stabilized the retained austenite structure at the interface. Due to the diffusion of carbon, the precipitates on Grade 22 side will dissolve leading to the formation of a zone of ferrite (marked as Y in Fig. 10) adjacent to X. The width of Y was much smaller ($\sim 20\text{ }\mu\text{m}$) when compared to the width of soft zone ($\sim 300\text{ }\mu\text{m}$), which forms in direct dissimilar welds between Grade 91 and Grade 22 ferritic steels for the same heat treatment condition (Ref. 5).

Conclusions

- A nickel-based interlayer of about 0.1 mm thickness was used to effectively control the formation of soft and hard zones in dissimilar weld cladding of ferritic steels.
- The hard zone was found to be absent in the Grade 91/ENiCrFe-3 interface. However, a zone of retained austenite of about 6- μm thickness formed in the interface of the Grade 22 and ENiCrFe-3 interlayer due to dilution during welding.
- Subsequent PWHT resulted in the formation of a soft zone adjacent to the retained austenite layer in the Grade 22/ENiCrFe-3 interface due to the diffusion of carbon.
- Width of the soft zone that forms adjacent to the zone of retained austenite was found to be much smaller than that observed in direct dissimilar welds without an interlayer for the same PWHT conditions.

Acknowledgments

The authors thank Baldev Raj, director IGCAR, P. R. Vasudeva Rao, director, MMG/IGCAR, and K. Bhanu Sankara Rao, associate director, MDCG/IGCAR, for their support and encouragement throughout the period of this project. The authors wish to thank S. Murugesan, PMD for his help in obtaining the X-ray diffraction pattern and S. K. Albert, MTD, for his useful suggestions during the course of the project.

References

1. Klueh, R. L., and Harries, D. R. 2001. *High Chromium Ferritic and Martensitic Steels for Nuclear Applications*. p. 5, ASTM.
2. Albert, S. K., Gill, T. P. S., Tyagi, A. K., Mannan, S. L., Kulkarni, S. D., and Rodriguez, P. 1997. Soft zone formation in dissimilar welds between two Cr-Mo steels. *Welding Journal* 76(3): 135-s to 142-s.
3. Kim, B. C., Ann, H. S., and Song, J. T. 1992. Analysis of carbon migration with post-weld heat treatment in dissimilar metal weld. *3rd Int. Conf. International Trends in Welding Science and Technology*. Eds. S. A. David and J. M. Vitek, pp. 307–314, Materials Park, Ohio: ASM International, Ohio.
4. Race, J. M., and Bhadeshia, H. K. D. H. 1992. Carbon migration across dissimilar steel welds. *ibid.* pp. 315–320.
5. Sudha, C., Terrance, A. L. E., Albert, S. K., and Vijayalakshmi, M. 2002. Systematic study of formation of soft and hard zones in dissimilar weldments of Cr-Mo steels. *J. Nucl. Mater.* 302: 193–205.
6. Buchmayer, B., and Kirkaldy, J. S. 1990. Preferential concentration and depletion of carbides after annealing of mismatched chromium alloy weldments. *Proc. Int. Symposium — Fundamentals and Applications of Ternary Diffusion*. Ed. G. R. Purdy, pp. 164–172, Pergamon Press, New York.
7. Celik, A., and Alsarhan, A. 1999. Mechanical and structural properties of similar and dissimilar steel joint. *Mater. Chara.* 43: 311–318.
8. Kucera, J., Vrestal, J., and Stransky, K. 1989. The influence of Ni-barrier on carbon redistribution in the steel weldments. *Defect and Diffusion Forum* 66–69: 1395–1400.
9. Golovanenko, S. A., and Konnova, I. Yu. 1972. Selecting interlayers for corrosion resistant bimetal. *Metal Science and Heat Treatment* 13(7-8): 570–575.
10. Emerson, R. W., Jackson, R. W., and Dauber, C. A. 1962. Transition joints between austenitic and ferritic steel piping for high-temperature steam service. *Welding Journal* 41: 385-s to 393-s.
11. You, Y.-Y., Shiue, R.-K., Shiue, R.-H., and Chen, C. 2001. The study of carbon migration in dissimilar welding of the modified 9Cr-1Mo steel. *J. Mater. Sci. Letters* 20: 1429 to 1432.
12. Jones, W. K. C. 1974. Heat treatment effect on 2CrMo joints welded with a nickel-base electrode. *Welding Journal* 53(5): 225-s to 231-s.
13. Slaughter, G. M., and Housley, T. R. 1964. The welding of ferritic steels to austenitic stainless steels. *Welding Journal* 43(10): 454-s to 460-s.
14. Bhaduri, A. K., Venkadesan, S., Rodriguez, P., and Mukunda, P. G. 1994. Transition metal joints for steam generators — An overview. *Int. J. Pressure Vessels and Piping* 58: 251–264.
15. Barford, J., and Probert, K. S. 1972. Interfacial effects in dissimilar steel joints. *Proc. Int. Conf. Welding Research Related to Power Plants*. Ed. L. M. Wyatt, pp. 412–424. MEP, London.
16. Viswanathan, R., Jaffee, R. I., and Dimmes, J. 1982. Dissimilar metal welds in power plants. *Proc. Conf. Joining Dissimilar Metals*. pp. 7–36. American Welding Society, Miami, Fla.
17. Gauzzi, F., and Missori, S. 1988. Microstructural transformations in austenitic-ferritic transition joints. *J. Mater. Sci.* 23: 782–789.

18. Parker, J. D., and Stratford, G. C. 1999. Review of factors affecting condition assessment of nickel-based transition joints. *Science and Technology of Welding and Joining* 4(1): 29–39.

19. Parker, J. D., and Stratford, G. C. 2000. Characterization of microstructures in nickel-based transition joints. *J. Mater. Sci.* 35: 4099–4107.

20. Bhaduri, A. K., Srinivasan, G., Gill, T. P. S., and Mannan, S. L. 1995. Effect of aging on the microstructure and tensile properties of alloy 800/9Cr-1Mo steel joint. *Int. J. Pressure Vessels and Piping* 61: 25–33.

21. Bhaduri, A. K., Venkadesan, S., Rodriguez, P., and Mukunda, P. G. 1991. Combined effects of postweld heat treatment and aging on Alloy 800/2.25Cr-1Mo steel joint. *Mater. Sci. Technol.* 7: 1051–1056.

22. Parker, J. D., and Stratford, G. C. 2001. The high-temperature performance of nickel-based transition joints - I. Deformation behaviour. *Mater. Sci. Engg.* A299: 164–173.

23. Li, C. C., Viswanathan, R., and Ryder, R. H. 1983. The microstructure and remaining life of dissimilar weldments after service in fossil fired boilers. *ASME Int. Conf. Advances in Life Prediction Methods*. Eds. D. A. Woodford, and J. R. Whitehead, pp. 315–325. ASME, New York.

24. King, J. F., Slaughter, G. M., and Sullivan, M. D. 1978. Ferritic steels for fast reactor steam generators. p. 476, London, BNES.

25. King, J. F., Sullivan, M. D., and Slaughter, G. M. 1977. Development of an improved stainless steel to ferritic steel transition joint. *Welding Journal* 56(11): 354-s to 358-s.

26. David, N. F. 1981. High-nickel joints unite dissimilar steels. *Welding Design and Fabrication* 54: 92–93.

27. Jang, C., Lee, J., Kim, J. S., and Jin, T. E. 2008. Mechanical property variation within Inconel 82/182 dissimilar metal weld between low-alloy steel and 316 stainless steel. *Inter. J. Pressure Vessels and Piping* 85: 635–646.

28. Gong, J. M., Jiang, Y., and Tu, S. T. 2004. Effect of carbon migration on creep properties of Cr5Mo dissimilar welded joints with Ni-based and austenitic weld metal. *Acta Metall. Sinica* (English Letters) 17(4): 560–568.

29. Kim, J. W., Lee, K., Kim, J. S., and Byun, T. S. 2009. Local mechanical properties of alloy 82/182 dissimilar weld joint between SA508 Gr.1a and F316 SS at RT and 320°C. *J. Nucl. Mater.* 384: 212 to 221.

30. Sudha, C., Thomas Paul, V., Terrance, A. L. E., Saroja, S., and Vijayalakshmi, M. 2006. Microstructure and microchemistry of hard zone in dissimilar weldments of Cr-Mo steels. *Welding Journal* 85(3): 71-s to 80-s.

31. Anand, R., Sudha, C., Karthikeyan, T., Terrance, A. L. E., Saroja, S., and Vijayalakshmi, M. 2009. Effectiveness of Ni-based diffusion barriers in preventing hard zone formation in ferritic steel joints. *J. Mater. Sci.* 44(1): 257–265.

32. Anand, R., Sudha, C., Karthikeyan, T., Terrance, A. L. E., Saroja, S., and Vijayalakshmi, M. 2008. Metal interlayers to prevent 'hard zone' formation in dissimilar weldments of Cr-Mo steels — A comparison between Cu, Co and Ni. *Trans. Indian Institute of Metals* 61(6): 483–486.

33. Orr, J., Beckitt, F. R., and Fawkes, G. D. 1978. *Ferritic Steels for Fast Reactor Steam Gen-*

erators. 91, London, BNES.

34. Parameswaran, P., Vijayalakshmi, M., Shankar, P., and Raghunathan, V. S. 1993. Influence of carbon content on microstructure and tempering behavior of 2¼Cr-1Mo steel. *J. Mater. Sci.* 28(20): 5426–5434.

35. Kindrachuk, V., Wanderka, N., Banhart, J., Mukherji, D., Del Genovese, D., and Rosler, J. 2008. Effect of rhenium addition on the microstructure of the superalloy Inconel 706. *Acta Materialia*. 56: 1609–1618.

36. Cullity, B. D. 1975. *Elements of X-ray Diffraction*. p. 394, Reading, Addison Wesley.

37. Krauss, G. 1980. *Principles of Heat Treatment of Steel*. p. 55, Ohio, ASM.

38. Capdevila, C., Caballero, F. G., and Garcia De Andres, C. 2002. Determination of Ms temperature in steels: A Bayesian neural network model. *ISIJ International* 42(8): 894–902.

39. Saroja, S., Vijayalakshmi, M., and Raghunathan, V. S. 1992. Influence of cooling rates on the transformation behavior of 9Cr-1Mo-0.07C steel. *J. Mater. Sci.* 27(9): 2389–2396.

40. Eisenhittenleute, V. D. 1993. *Steel: A Handbook for Materials Research and Engineering* Vol. 2. p. 400, Berlin, Springer Verlag.

Appendix

The procedure adopted to arrive at the microchemistry of carbides is discussed in detail below.

1) Based on the analysis of SAD pattern, the type of carbide is identified (Eg. $M_{23}C_6$)

2) The X-ray spectra from the carbides

are analyzed using the procedure of normalizing the contents of the elements, Fe, Cr, and Mo except carbon. Thin foil approximation was used and absorption correction was applied.

3. The result of the above step does not give the composition of the carbide but the content of Fe, Cr, and Mo in 'M' in the carbide (Eg. $M_{23}C_6$).

4. Since the formula of the carbide and the specific ratio of the content of the three elements are known, the stoichiometry of the carbide is calculated as follows: For Eg,

$$x_{Fe} = \frac{\%Fe \text{ in } M}{100} \times 23 \text{ (in this case)}$$

5. Based on the evaluated stoichiometry of the carbide, the weight-percentage of each element was estimated using the equation

$$wt - \% \text{ of } Fe = \frac{X_{Fe} A_{Fe}}{(X_{Fe} A_{Fe} + X_{Cr} A_{Cr} + X_{Mo} A_{Mo} + X_C A_C)}$$

Where A_{Fe} , A_{Cr} , A_{Mo} , and A_C refer to the atomic weight of Fe, Cr, Mo, and C, respectively.

The statistical error for 99% confidence limit (± 2) is about $\pm 2\%$ for Fe, $\pm 4\%$ for Cr, and $\pm 6\%$ for Mo.

Call for Papers

**JOM-16, 16th Int'l Conf. on the Joining of Materials, and
7th Int'l Conf. on Education in Welding, ICEW-7**
May 10–13, 2011, Helsingør, Denmark

Deadline for receipt of abstracts is Nov. 15, 2010

Topics of interest include all aspects of developments in joining and materials technology, especially:

Recent developments in welding, soldering, and brazing.

Advances in materials, metallurgy, and weldability.

Applications with close relevance to industry's needs including oil, gas, and power generation.

Weld quality, structural properties, and environmental considerations.

Education, training, and qualification and certification of welding personnel.

Process monitoring, sensors, and control.

Mathematical modeling and simulation.

JOM Institute

Gilleleje Strandvej 28, DK-3250, Gilleleje, Denmark
jom_aws@post10.tele.dk, or call +45 48355458